Defect Cores Investigated by X-Ray Scattering close to Forbidden Reflections in Silicon

M.-I. Richard[1,2] and T. H. Metzger[1]

[1]*ESRF, 6 rue Jules Horowitz, BP220, F-38043 Grenoble Cedex, France*
[2]*Département de Recherche Fondamentale sur la Matiére Condensée/SP2M/NRS, CEA Grenoble,
17 Avenue des Martyrs, F-38054 Grenoble Cedex 9, France*

V. Holý

Faculty of Mathematics and Physics, Charles University, Ke Karlovu 5, 121 16 Prague, Czech Republic

K. Nordlund

Accelerator Laboratory, P.O. Box 43, FIN-00014 University of Helsinki, Finland
(Received 30 July 2007; published 30 November 2007)

A new x-ray scattering method is presented making possible the detection of defects and the investigation of the structure of their cores. The method uses diffuse x-ray scattering measured close to a forbidden diffraction peak, in which the intensity scattered from the distorted crystal lattice around the defects is minimized. As a first example of this nondestructive method we demonstrate how the local compression of the extra {111} double planes in extrinsic stacking faults in Si can be probed and quantified using a continuum approach for the simulation of the displacements. The results of the theory developed are found to be in very good agreement with atomistic simulations and experiments.

In silicon implantation, the interaction of defects and impurities play a crucial role in the doping of silicon [1,2]. In device fabrication, an important issue is that the nanostructure interfaces must be kept free of defects in order to obtain the desired electronic properties [3]. For instance, misfit dislocations at interfaces cause increases in the off-leakage current of metal-oxide-semiconductor field effect transistors (MOSFETs) [4]. The most important extended defects observed in such systems are stacking faults, "311" defects, and perfect dislocation loops [5]. Transmission electron microscopy (TEM) is a technique of choice to determine the structure, nature, and location of these defects. However, TEM experiments remain a destructive analysis. Diffuse x-ray scattering is a well-established method for the investigation of defects in crystals [6,7]. This method is based on the measurement of the distribution of the scattered intensity I in reciprocal space, i.e., as a function of the scattering vector $\mathbf{Q} = \mathbf{K}_f - \mathbf{K}_i$, where $\mathbf{K}_{i,f}$ are the wave vectors of the primary and scattered radiations. The measured intensity distribution $I(\mathbf{Q})$ is a coherent superposition of two contributions—scattering from the defects core and scattering from the deformed lattice around the defect (displacement-field scattering; see also Ref. [8]). Usually, the displacement-field scattering close to allowed Bragg peaks (the Huang scattering) is used for the defect investigation. However, close to an allowed Bragg peak, the contribution of the defect cores is very weak due to very small volumes of the defect cores and to the high contribution of the Huang scattering, so that the investigation of the structure of the defect core is difficult or only indirect, via the measurement of the displacement field *around* the defect core. Not only diffuse scattering measurements around allowed reflections but

also high-resolution TEM (HRTEM) experiments toil in observing the atomic displacement field of the atoms in the core of defects [9].

In this Letter, we present a novel x-ray method how to study the defect cores *directly*. Recently, A. Malachias [10] reported on the idea to use forbidden reflection to detect the formation of atomic ordering inside SiGe nanostructures. In contrary to that work, we use a forbidden reflection for the suppression of the displacement-field scattering so that the scattered intensity consists mainly of the core scattering. Using this method, we investigate the structure of the cores of extrinsic stacking faults created in Si crystal after amorphizing ion implantation and subsequent annealing. We probe the small and local deformation field inside the defect cores in determining the distance Δ between two adjacent {111} planes (denoted by Aa in [11]) creating the core of the stacking fault and we compare this distance with the results of atomistic simulations.

Restricting ourselves to the kinematical approximation and assuming only one type of atoms present in the crystal (Si atoms, in our case), the amplitude of the wave scattered by a distorted crystal is

$$E(\mathbf{Q}) = f(\mathbf{Q})\left[\sum_{n,s} e^{-i\mathbf{Q}.(\mathbf{R}_n+\mathbf{r}_s)}e^{-i\mathbf{Q}.\mathbf{u}(\mathbf{R}_n+\mathbf{r}_s)} + \sum_c e^{-i\mathbf{Q}.\mathbf{R}_c}\right],$$
(1)

where the sum $\sum_n$ runs over the unit cells (with nondisturbed positions $\mathbf{R}_n$), $\sum_s$ is over the atoms within one unit cell, having the nondisturbed positions $\mathbf{r}_s$. Because of the defects, the atoms are displaced from their ideal positions by $\mathbf{u}(\mathbf{R}_n + \mathbf{r}_s)$, $f(\mathbf{Q})$ is the atomic scattering factor (assumed not affected by the disturbance). The second term in

Eq. (1) expresses the contribution of extra atoms (atoms of the defect cores) in the positions $\mathbf{R}_c$.

Let us assume that the investigated crystal contains small defects in noncorrelated random positions. We restrict ourselves to weak defects (see the defect classification in Ref. [6]). After averaging over random defect positions we find that the diffuse part of the scattered intensity is a coherent superposition of two contributions $I(\mathbf{Q}) \sim |E_1(\mathbf{Q}) + E_2(\mathbf{Q})|^2$, where E_1 describes the scattering from the displacement field around a single defect and $E_2 = f(\mathbf{Q})\sum_c \Omega(\mathbf{R}_c) \exp(-i\mathbf{Q}.\mathbf{R}_c)$ is the scattering from the defect core, $\Omega(\mathbf{r})$ is the shape function of a single defect core (unity in the core and zero outside it). Expressing the sum $\sum_n$ over the lattice points by the sum $\sum_{\mathbf{g}}$ over the reciprocal lattice points (RELPs) $\mathbf{g}$ we obtain the displacement-field term in the form

$$E_1(\mathbf{Q}) = \frac{f(\mathbf{Q})}{V_{\text{cell}}} \sum_{\mathbf{g}} F_0(\mathbf{g})\psi(\mathbf{Q} - \mathbf{g}, \mathbf{Q}), \qquad (2)$$

where $F_0(\mathbf{g}) = \sum_s e^{-i\mathbf{g}\cdot\mathbf{r}_s}$ the structure factor of a *nondeformed* unit cell, $V_{\text{cell}} = a^3$ is the volume of the unit cell, and

$$\psi(\mathbf{Q} - \mathbf{g}, \mathbf{Q}) = \int d^3\mathbf{r}\, e^{-i(\mathbf{Q}-\mathbf{g})\cdot\mathbf{r}}[e^{-i\mathbf{Q}\cdot\mathbf{v}(\mathbf{r})} - 1], \qquad (3)$$

$\mathbf{v}(\mathbf{r})$ is the displacement field around a *single* defect. According to Eq. (2), the intensity of the displacement-field scattering in a given point $\mathbf{Q}$ in reciprocal space is a coherent superposition of contributions centered in various RELPs $\mathbf{g}$. If we can neglect the overlapping of the contributions from different $\mathbf{g}$'s, in the sum $\sum_{\mathbf{g}}$ only the term with minimum deviation $\mathbf{Q} - \mathbf{g}$ is not negligible (say, the term $\mathbf{g} = \mathbf{h}$). If, in addition, the diffraction $\mathbf{h}$ is forbidden [i.e., $F_0(\mathbf{h}) = 0$; 200 in Si, for instance], the displacement-scattering term can be neglected and the diffuse scattering stems only from the defect cores. Even if this overlapping cannot be neglected, the E_1 contribution to the diffusely scattered intensity close to a forbidden RELP $\mathbf{h}$ is suppressed and the intensity is mainly influenced by the core term, i.e., by the atomic positions in the defect cores.

In order to demonstrate the sensitivity of the scattered intensity to the defect core structure, we have simulated the intensity scattered from a Si crystal containing randomly distributed small circular stacking faults; the faults lie in {111} planes having the Burgers vector $\mathbf{b} = 1/3\langle 111 \rangle$ perpendicular to the planes (the Frank loops [11]). For the sake of simplicity, we have assumed that all the loops have the same radius R_0. For Huang scattering, i.e., for $|\mathbf{Q} - \mathbf{h}| \ll |\mathbf{h}|$, the asymptotic long-range deformation field of a defect $\lim_{|\mathbf{r}|\to\infty}\mathbf{v}(\mathbf{r})$ plays a role. Such an asymptotic field has been derived by means of the elastic Green-function approach [12] and it can be expressed quite easily by means of a double-force tensor of the defect. However, in our simulation the asymptotic expression is not sufficient, since we are dealing with the intensity distribution far

away from a RELP, where the displacement field $\mathbf{v}(\mathbf{r})$ in the vicinity of the defect becomes important. Therefore, we have used a more exact Burgers formula [11] describing the displacement field of a fault loop also in its close neighborhood. It has been demonstrated in Ref. [13] that the intensity of diffuse x-ray scattering calculated by this formula compares well with the result of atomistic simulations. The core of a Frank loop consists of two extra {111} planes (denoted A and a in [11]), having the nominal distance $\Delta_0 = a\sqrt{3}/4$. The atoms in these planes are arranged in a hexagonal array; the distance of nearest atoms in the plane is $a\sqrt{2}/2$. From symmetry considerations it follows that the reciprocal-space distribution of the scattered intensity $I(\mathbf{Q})$ is concentrated along lines $\langle 111 \rangle$ perpendicular to the loop planes.

In Fig. 1 we have plotted the distribution of the scattered intensity calculated along the [111] direction perpendicular to the fault plane around the forbidden RELP $\mathbf{h} = [200]$, in which $\mathbf{q} \equiv \mathbf{Q} - \mathbf{h} = 0$. From the figure it follows that the intensity $I(\mathbf{Q})$ around the forbidden RELP $\mathbf{h} = [200]$ very sensitively depends on small changes in the plane distance Δ, while the intensity close to an allowed RELP (311 or 111, for instance) is almost Δ independent. Figure 1 illustrates the origin of this behavior. Around an allowed RELP the term $E_1(\mathbf{Q})$ is dominant and the core term $E_2(\mathbf{Q})$ can be neglected. Around a forbidden RELP $\mathbf{h}$, only more distant allowed RELPs $\mathbf{g} \neq \mathbf{h}$ contribute to $E_1(\mathbf{Q})$ and the resulting term $E_1(\mathbf{Q})$ is comparable or even smaller than the core term $E_2(\mathbf{Q})$. A small change in Δ only slightly affects the intensity $|E_2|^2$ of the core term but it changes substantially its phase and also the total intensity around the forbidden RELP, being proportional to $|E_1(\mathbf{Q}) + E_2(\mathbf{Q})|^2$.

We have used this approach for the investigation of the core structure of small stacking faults generated in Si(001) by Xe-implantation and subsequent annealing [14]. The
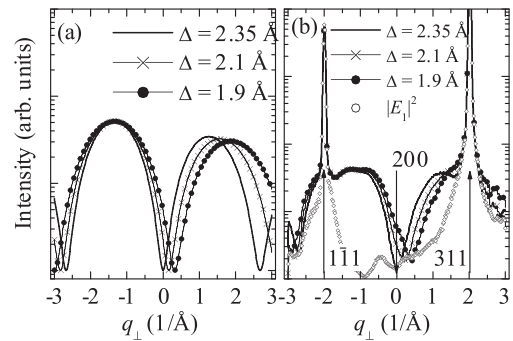

FIG. 1. The distribution of diffusely scattered intensity from circular stacking faults calculated along the line [111] perpendicular to the loop plane. The loop radius is $R_0 = 30$ nm, the point $q_\perp = 0$ corresponds to the forbidden RELP 200. In figure (a), the contributions of the defect cores are plotted for various distances Δ of the defect (111) planes; figure (b) shows the total intensities as well as the displacement-field contribution $|E_1|^2$ that does not depend on Δ (points).

annealing results in the formation of extended defects in Si(001) in a depth of about 100 nm, i.e., faulted extrinsic dislocation loops. The diffuse x-ray scattering has been measured on the beamline ID01 at ESRF, Grenoble using the x-ray energy of 8 keV in the grazing-incidence geometry, in which the diffraction vector $\mathbf{h} = [200]$ was parallel to the sample surface. We kept constant the incidence angle to 0.35°, i.e., 0.13° above the critical angle of total external reflection. The scattered radiation was collected by a linear detector perpendicular to the sample surface. A three-dimensional intensity distribution $I(\mathbf{Q})$ around the 200 reciprocal lattice point was recorded. The diffuse scattering was concentrated in intensity streaks along $\langle 111 \rangle$ directions visible in Fig. 2. Because of the grazing-incidence geometry used, only half of reciprocal space above the sample horizon ($Q_z > 0$) can be covered. The full width at half maximum (FWHM) $\delta q_{\parallel}$ of the streak cross-section is $\delta q_{\parallel} = 2\pi/(2R_0)$. From the fit the mean radius $R_0 = (30 \pm 2)$ nm of the faults follows.

The intensity distribution along the streaks $I(q_{\perp})$ is plotted in Fig. 3. The intensity has been corrected by the polarization factor and beam footprint [15]. Here $q_{\perp}$ is the coordinate of $\mathbf{q}$ along the trajectory depicted in Fig. 2 (see white dashed lines); $q_{\perp} = 0$ corresponds to the forbidden RELP $\mathbf{h} = [200]$. We have fitted this distribution to the theory described above; in the fit we relied on only one free parameter Δ; from the fit $\Delta = (2.1 \pm 0.2)$ Å follows. Calculating the scattered intensity, we took into account the defect-free surface layer mentioned above, and the dependence of the irradiated sample depth L on the incidence and exit angles. The correspondence of the measured and fitted intensity distribution is good (see Fig. 3, full line).

It is worthy to note that the diffusely scattered intensity cannot be explained only by the core scattering, even if the nearest RELP is forbidden. Since the defects are very thin in the direction perpendicular to the loop plane, the extension of the $|E_1(\mathbf{Q})|^2$ term in this direction is comparable to the distance of nearest RELPs, and this term is not negligible even around a forbidden RELP. If we neglect completely $E_1(\mathbf{Q})$, the asymmetry of the experimental intensity distribution around 200 can be explained only by nonrealistically small value of Δ. As demonstrated by previous works on a different system [16], we show that the local information is not only encoded in the diffuse scattering near forbidden reflection. The scattering around several allowed reciprocal-space points need to be taken into account to analytically simulate and quantify the defect cores.

We have compared the simulated intensity distribution with the result of atomistic simulations [13]. An extrinsic stacking fault was created by adding an extra double (111) atom plane in the center of a large simulation cell, with a length of $20\frac{1}{2}[110]a$ (a is the lattice constant). Because of computational limitation, the size of the defect is chosen 4 times smaller than the average measured stacking fault size. Using the positions of atoms following from the atomistic simulations, we have calculated the scattered intensity directly using Eq. (1), plotted as the dashed line in Fig. 3. In the simulation, we averaged the scattered intensity over all four possible {111} orientations of a stacking fault. We studied size effects and show that the stacking fault size has no impact on the shape of the fault's core signal. The dashed line in Fig. 3 exhibits a small sharp maximum also in the forbidden 200 point ($q_{\perp} = 0$). This maximum is caused by the size truncation of the crystal that was included in the atomistic simulation. Except for this maximum, the correspondence between the measured and simulated curves is very good.

Figure 4 schematically depicts the sequence of (111) layers and positions of the atoms obtained by the atomistic
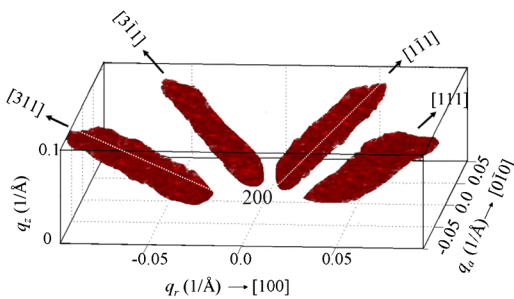

FIG. 2 (color online). Reciprocal-space distribution of the scattered intensity measured in forbidden grazing-incidence diffraction $\mathbf{h} = [200]$; the white dashed lines denote the trajectory along which the line scan in Fig. 3 was measured. $q_{r,a}$ are the radial and angular coordinates parallel and perpendicular to $\mathbf{h}$, respectively. q_z is the out-of-plane coordinate. The (111) planar defects are two-dimensional objects in real space; their Fourier Transform yields 1D intensity rods perpendicular to the (111) planar defects. The rods are thus along the $\langle 111 \rangle$ directions, perpendicular to the four possible {111} fault planes.
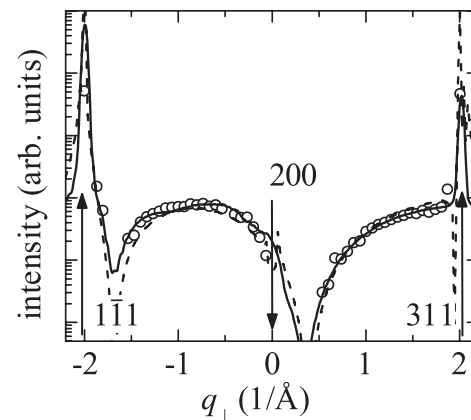

FIG. 3.   Distribution of the measured intensity (points) along the trajectory denoted in Fig. 2, along with its theoretical fit using the Burgers formula (full line) and atomistic simulations for the displacement field (dashed line).
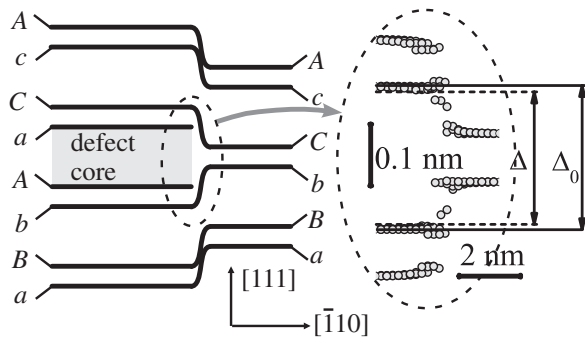
P H Y S I C A L   R E V I E W   L E T T E R S

FIG. 4. Schematic sketch of the stacking of the sequence of (111) layers, the defect core (gray rectangle) is represented by a pair of inserted Aa layers. In the inset, the atomic positions are plotted around the edge of the defect core, following from the atomistic simulations. The full horizontal lines represent the ideal distance Δ_0 of the core planes, the dashed lines denote the distance Δ of these plane following from the fit of the measured intensities (full line in Fig. 3).

simulation in a close vicinity of the defect core (a double layer denoted Aa) inserted between the double layers Bb and Cc of the crystal matrix. For clarity, we have plotted only the atoms with small coordinates along $[\bar{1}\,\bar{1}\,2]$. Here we compare the ideal distance Δ_0 of the Aa layers creating the defect core (denoted by a pair of straight full lines) with the distance Δ following from the fit of the measured intensity distribution (dashed straight lines). From the atomistic simulation it follows that the atoms in the defect core close to its periphery are displaced along the [111] Burgers vector so that the inserted Aa discs are not plane. Most likely, this distortion at the edge of the defect core is the reason of the difference between the measured intensity distribution and the intensity profile simulated using the theory in Eqs. (1)–(3) (full line in Fig. 3), in which no distortion of the inserted Aa planes was assumed. Nevertheless, the value of Δ obtained from the fit corresponds well to the mean distance between the atoms in the A and a core planes in [111] direction.

In summary, we have demonstrated that diffuse x-ray scattering around a forbidden reciprocal lattice point is well suited for the study of the cores of extrinsic stacking faults in Si. The diffuse scattering from the distorted neighborhood of the defects is fairly suppressed in this case which makes it possible to study directly the atomic structure of the defect cores. From the comparison of the measured intensity with a simulation based on the continuum displacement model we have revealed a compression of the {111} planes in the defect cores. This finding was supported by atomistic simulations. Thus, diffuse x-ray scattering near forbidden reflection appears as a fine, unique and destruction-free technique to detect stacking

faults and characterize their small compression in the core. This x-ray method can be easily combined with *in situ* growth [17] to detect, for instance, the formation of stacking faults inside nanostructures. The method can also be used for other defects, as long as the lattice of the defect cores contributes to the scattered intensity close to a diffraction that is forbidden for the host lattice. The signature in the x-ray scattering profile near forbidden reflections will depend on the nature of the defects.

[1] E. Chason, S. T. Picraux, M. Poate, J. O. Borland, M. I. Current, T. Diaz de la Rubia, D. J. Eagleasham, O. W. Holland, M. E. Law, C. W. Magee, J. W. Mayer, J. Melngailis, and A. F. Tasch, J. Appl. Phys. **81**, 6513 (1997).

[2] L. Capello, T. H. Metzger, V. Holý, M. Servidori, and A. Malachias, J. Appl. Crystallogr. **39**, 571 (2006).

[3] J. Stangl, V. Holý, and G. Bauer, Rev. Mod. Phys. **76** 725 (2004).

[4] J. G. Fiorenza, G. Braithwaite, C. W. Leitz, M. T. Currie, J. Yap, F. Singaporewala, V. K. Yang, T. A. Langdo, J. Carlin, M. Somerville, A. Lochtefeld, H. Badawi, and M. T. Bulsara, Semicond. Sci. Technol. **19**, L4 (2004).

[5] K. Nordlund, J. Appl. Phys. **91**, 2978 (2002).

[6] M. A. Krivoglaz, *X-Ray and Neutron Diffraction in Nonideal Crystals* (Springer, New York, 1996).

[7] U. Pietsch, V. Holý, and T. Baumbach, *High-Resolution X-Ray Scattering: From Thin Films to Lateral Nanostructures* (Springer, New York, 2004).

[8] H. Trinkaus, Phys. Status Solidi B **51**, 307 (1972); **54**, 209 (1972).

[9] A. Claverie (private communication).

[10] A. Malachias, T. U. Schülli, G. Medeiros-Ribeiro, L. G. Cancado, M. Stoffel, O. G. Schmidt, T. H. Metzger, and R. Magalhães-Paniago, Phys. Rev. B **72**, 165315 (2005).

[11] J. P. Hirth and J. Lothe, *Theory of Dislocations* (Krieger, Malabar, Florida, 1992).

[12] P. H. Dederichs, Phys. Rev. B **1**, 1306 (1970); **4**, 1041 (1971).

[13] K. Nordlund, U. Beck, T. H. Metzger, and J. R. Patel, Appl. Phys. Lett. **76**, 846 (2000).

[14] L. Capello and T. H. Metzger, Mater. Sci. Eng. B **114**, 77 (2004).

[15] E. Vlieg, J. Appl. Crystallogr. **30**, 532 (1997).

[16] H. Dosch, J. Peisl, and B. Dorner, Phys. Rev. B **35**, 3069 (1987).

[17] http://www.esrf.eu/UsersAndScience/Experiments/CRG/BM32.